

Optimistic Query Routing in Clustering-based Approximate Maximum Inner Product Search

SEBASTIAN BRUCH, Northeastern University, USA

ADITYA KRISHNAN, Pinecone, USA

FRANCO MARIA NARDINI, ISTI-CNR, Italy

Clustering-based nearest neighbor search is an effective method in which points are partitioned into geometric shards to form an index, with only a few shards searched during query processing to find a set of top- k vectors. Even though the search efficacy is heavily influenced by the algorithm that identifies the shards to probe, it has received little attention in the literature. This work bridges that gap by studying routing in clustering-based maximum inner product search. We unpack existing routers and notice the surprising contribution of optimism. We then take a page from the sequential decision making literature and formalize that insight following the principle of “optimism in the face of uncertainty.” In particular, we present a framework that incorporates the moments of the distribution of inner products within each shard to estimate the maximum inner product. We then present an instance of our algorithm that uses only the first two moments to reach the same accuracy as state-of-the-art routers such as SCANN by probing up to 50% fewer points on benchmark datasets. Our algorithm is also space-efficient: we design a sketch of the second moment whose size is independent of the number of points and requires $O(1)$ vectors per shard.

CCS Concepts: • **Information systems** → **Retrieval models and ranking**.

Additional Key Words and Phrases: maximum inner product search, clustering-based nearest neighbor search, query routing, sketching, optimism principle

1 INTRODUCTION

A fundamental operation in modern information retrieval and database systems is what is known as Nearest Neighbor search or top- k vector retrieval [8]. It is defined as follows: Given a collection \mathcal{X} of m data points in \mathbb{R}^d , we wish to find the k closest points to a query $q \in \mathbb{R}^d$, where closeness is determined by some notion of vector similarity or distance. In this work, we focus exclusively on inner product as a measure of similarity, leading to the following formal definition known as Maximum Inner Product Search (MIPS):

$$\mathcal{S} = \arg \max_{u \in \mathcal{X}}^{(k)} \langle q, u \rangle. \quad (1)$$

Unsurprisingly, it is often too difficult to solve this problem exactly within a reasonable time budget, especially as m or d increases. As such, the problem is often relaxed to its approximate variant, where we tolerate error in the retrieved set to allow faster query processing. This approximate version of the problem is aptly named Approximate Nearest Neighbor (ANN) search, whose effectiveness is characterized by the fraction of true nearest neighbors recalled in the retrieved set: $|\tilde{\mathcal{S}} \cap \mathcal{S}|/k$, where $\tilde{\mathcal{S}}$ is the set returned by an ANN algorithm. We call this metric *recall*, or equivalently, *accuracy*.

1.1 Clustering-based ANN search

ANN algorithms come in various flavors, from trees [6, 11], LSH [16], to graphs [18, 25]. Refer to [8] for a thorough review of this subject. The method relevant to this work is the clustering-based approach, also known as Inverted File (IVF) [19], which has proven effective in practice [4, 5, 9, 10, 13]. In this paradigm, data points are partitioned into C shards using a clustering function

Authors’ addresses: Sebastian Bruch, s.bruch@northeastern.edu, Northeastern University, Boston, MA, USA; Aditya Krishnan, aditya.krishnan94@gmail.com, Pinecone, New York, NY, USA; Franco Maria Nardini, ISTI-CNR, Pisa, Italy, francomaria.nardini@isti.cnr.it.

$\zeta : \mathbb{R}^d \rightarrow [C]$ on X . A typical choice for ζ is the KMeans algorithm with $C = O(\sqrt{m})$. This forms the *index* data structure.

Accompanying the index is a *routing* function $\tau : \mathbb{R}^d \rightarrow [C]^\ell$. It takes a query q and returns ℓ shards that are more likely to contain its nearest neighbors. A common router is as follows:

$$\tau(q) = \arg \max_{i \in [C]}^{(\ell)} \langle q, \mu_i \rangle, \quad (2)$$

where μ_i is the *mean* of the i -th shard.

Processing a query q involves two *independent* subroutines. The first stage, which we call “routing,” obtains a list of ℓ shards using $\tau(q)$, and the subsequent step, “scoring,” computes inner product between the query and the points in the union of the selected shards. While a great deal of research has focused on scoring step [3, 14, 19–21, 28, 35], routing has received relatively little attention. This work turns squarely to the first step: Routing queries to shards.

Before we proceed further, we wish to emphasize the following point: In a clustering-based ANN system, we can select a routing protocol to choose shards, *independently* of the scoring algorithm that evaluates the chosen shards. For example, we may route queries to shards (i.e., decide which shards to probe) using Equation (2) or using our novel router to be introduced later. This choice has no algorithmic bearing on the scoring phase whatsoever. In other words, the scoring stage can perform a linear scan of the chosen shards, or it may compute inner products using Product Quantization (PQ) [19], or it may further index and search each shard using a graph ANN algorithm [18, 25]. All these choices are independent of the type of router utilized in the earlier stage. This is indeed one of the advantages of a clustering-based ANN search system.

That independence simplifies the evaluation of different routing protocols: By independence and the additivity of latency, any efficiency savings achieved by a router translates directly into efficiency savings, of the same magnitude, for the end-to-end retrieval system (i.e., routing followed by scoring). For instance, if two routers lead to the same end-to-end recall, but one does so at a substantially lower latency, its latency savings will be reflected in its end-to-end query latency. As a result, we can fix the scoring stage across our experiments (to an exact linear scan, e.g.), and examine routers in isolation to compare their accuracy, latency, and other characteristics.

1.2 The importance of routing

The historical focus on the scoring phase makes sense. Even though the routing step narrows down the search space, selected shards may nonetheless contain a large number of points. It is thus imperative that the scoring stage be efficient and effective.

We argue that the oft-overlooked routing step is important in its own right. The first and obvious reason is that, the more accurately¹ a router chooses a subset of shards, the fewer data points the scoring stage must examine. For example, if shards are balanced in size, access to an oracle router (i.e., one that identifies the shard with the true nearest neighbor) means that the scoring stage must only compute inner products for m/C points to find the top-1 point.

The second reason pertains to scale. As collections grow in size and dimensionality, it is often infeasible to keep the entire index in memory, in spite of compression techniques such as PQ. Much of the index must therefore rest on secondary storage—in particular, cheap but high-latency storage such as disk or blob storage—and accessed only when necessary. That line of reasoning has led to the emergence of disk-based graph indexes [17, 18, 32] and the like.

Translating the same rationale to the clustering-based paradigm implies that shards rest outside of the main memory, and that when a router identifies a subset of shards, the scoring stage must fetch

¹We quantify the accuracy of a router as the ANN recall in a setup where the scoring stage performs a linear scan over the identified shards. As such, the only source of ANN error is the routing procedure, rather than inner product computation.

those shards from storage for further processing. This paradigm has gained traction in real-world vector database systems.² This is the context in which we present our research: Storage-backed, clustering-based ANN search systems.

In this framework, a more accurate router lowers the volume of data that must be transferred between storage and memory. That has several consequences including a lower utilization of the storage bandwidth per query, as well as a lower consumption of in-memory cache space per query, thereby improving retrieval throughput.

1.3 An illustrative example

Interestingly, depending on operational factors such as query load, storage I/O bandwidth, data transfer rate, and memory utilization, it would be acceptable for the routing stage to be more computationally expensive as long as it identifies shards more accurately. Let us consider an illustrative example to support this statement and, in fact, motivate our research.

Consider Natural Questions [23] embedded with ADA-002³ denoted by NQ-ADA2. It contains 2.7 million 1,536-dimension points. When clustered with KMeans, each shard contains about 1,650 points, and is 1MB in size, if compressed with 4-bit PQ codebooks—a common configuration.

Next, consider a commercial machine: AWS c5.xlarge (with 4 vCPUs and 8GB of memory). Using 4 threads, transferring 4MB of data from blob storage (hosted on Amazon’s own S3) to main memory has an average latency of 45 milliseconds (ms).⁴

Given this setup, fetching 16 NQ-ADA2 shards from blob storage and downloading them to the machine’s main memory takes 180ms (P50 latency). On this same machine, routing using Equation (2) takes 0.76ms. As such, so long as a more complex router can achieve the same accuracy as Equation (2) by fetching 16 fewer shards, but by introducing a computational latency of no greater than roughly 179ms, the overall efficiency of the query processor improves. As we will show later, our router on the same dataset with the same configuration takes only about 10.1ms to route queries to shards, leading to a saving of 170.6ms per query in the given example.

As this example illustrates, a storage-backed, clustering-based ANN search system offers a trade-off space between not just accuracy and speed, but also other efficiency factors such as I/O bandwidth, and memory and cache utilization. This opens the door to more nuanced research. Our work is a step in that direction.

1.4 Existing routers and the role of optimism

As we argued, routing accuracy is increasingly relevant. Surprisingly, with the exception of one recent work that explores supervised learning-to-rank for routing [33], the few existing unsupervised routers take the naïve form of Equation (2).

Take Equation (2) as the most prominent example. What we refer to as the **MEAN** router summarizes each shard with its mean point (i.e., μ_i for shard i). This is not an unreasonable choice as the mean is the minimizer of the sum of squared deviations from the mean, and is, in fact, natural if KMeans is the clustering algorithm ζ .

Another common router, which we call **NORMALIZEDMEAN**, belongs to the same family, but its shard representatives are the L_2 -normalized means, rather than the unnormalized mean vectors:

$$\tau(q) = \arg \max_{i \in [C]}^{(\ell)} \left\langle q, \frac{\mu_i}{\|\mu_i\|_2} \right\rangle. \quad (3)$$

²See, for example, <https://turbopuffer.com/blog/turbopuffer> and <https://www.pinecone.io/blog/serverless-architecture/#Pinecone-serverless-architecture>.

³<https://openai.com/index/new-and-improved-embedding-model/>

⁴See <https://github.com/dvassallo/s3-benchmark> for an independent and comprehensive benchmark.

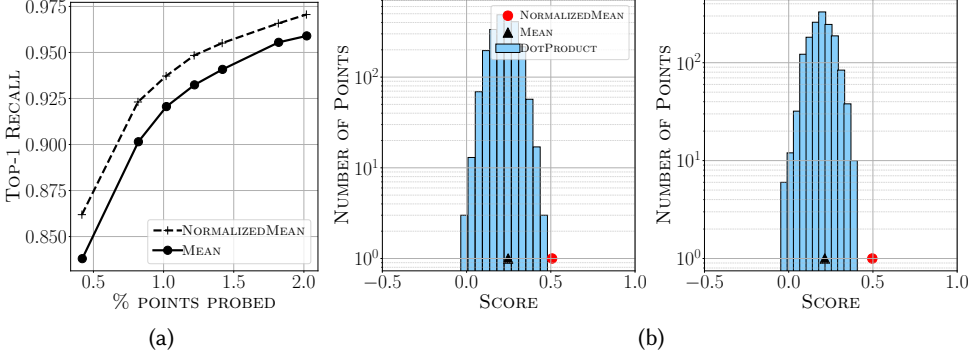


Fig. 1. (a) Top-1 recall vs. percentage of points probed on TEXT2IMAGE where points have varying norms; (b) Distribution of inner products between a shard and a query on GloVe. Overlaid are scores computed by MEAN and NORMALIZEDMEAN.

This formulation is inherited from the familiar *Spherical* KMeans [12], which is identical to standard KMeans except that, at the end of every iteration, cluster centroids are normalized. Because we can assume that $\|q\|_2 = 1$ without loss of generality, it is easy to see that Equation (3) routes by the angle between q and the mean vectors.

Intuitively, NORMALIZEDMEAN seems appropriate for ANN search over a sphere: When norms are constant, all that matters in Equation (1) is the angle between q and data points, rendering it reasonable to rank shards by the angle between their mean and q .

Intriguingly, in many circumstances that deviate from that situation, NORMALIZEDMEAN performs more accurately than the MEAN router, as evidenced in Figure 1(a). Let us unpack this phenomenon.

Consider a query point q and a single shard \mathcal{P} with mean μ . We visualize in Figure 1(b) the distribution of inner products between q and every point in \mathcal{P} . Overlaid is the inner product between q and the mean of points in \mathcal{P} , as well as their normalized mean. We observe that $\langle q, \mu / \|\mu\|_2 \rangle$ lands in the right tail of the distribution.

That is not surprising for the case where $\|u\|_2 = 1$ for all $u \in \mathcal{P}$. Clearly $\|\mu\|_2 \leq 1$, so that $\langle q, \mu / \|\mu\|_2 \rangle = \langle q, \mu \rangle / \|\mu\|_2 \geq \langle q, \mu \rangle$; the NORMALIZEDMEAN router amplifies the MEAN router by a factor of $1 / \|\mu\|_2$. What is interesting, however, is that the magnitude of this “boost” correlates with the variance of the data within \mathcal{P} : The more concentrated \mathcal{P} is around the direction of its mean, the closer the mean is to the surface of the sphere, making $\|\mu\|_2$ larger, so that NORMALIZEDMEAN applies a smaller amplification to $\langle q, \mu \rangle$. The opposite is true when points are spread out: shards with a higher variance receive a larger lift by the NORMALIZEDMEAN router!

There are a few caveats. First, it is hard to explain the behavior on point sets with varying norms (i.e., where $\|u\|_2 \neq 1$). Second, as we observe in Figure 1(b), NORMALIZEDMEAN aggressively overestimates. Nonetheless, the insight that a router’s score for a shard can be influenced by the shard’s variance is worth exploring.

Let us summarize our observation. The estimate given by NORMALIZEDMEAN paints an *optimistic* picture of what the maximum inner product between q and points in \mathcal{P} could be. Contrast that with the MEAN router, which is naturally a *conservative* estimate.

We investigate the ramifications of that insight. In particular, the research question we wish to study is whether a more principled approach to designing optimistic routers can lead to more accurate routing decisions on vector sets with variable norms. The nature of this question is not

unlike those asked in the online learning literature [24], so it is not surprising that our answer to this question draws from the “principle of optimism in the face of uncertainty.”

1.5 Contributions and outline

We apply the Optimism Principle to routing in clustering-based MIPS. Our formulation, presented in Section 2, rests on the concentration of the inner product distribution between a query q and a set of points in the same shard. In particular, we estimate a score, θ_i , for the i -th shard such that, with some confidence, the maximum inner product of q with points in that shard is at most θ_i . Shards are then ranked by their score for routing. Notice that, when $\theta_i = \mu_i$, we recover the MEAN router, and when $\theta_i > \mu_i$ routing is optimistic with the confidence parameter determining the degree of optimism.

Building on our proposed formalism of an optimistic router, we outline a general framework that can incorporate as much information as is available about the data distribution to estimate the aforementioned scores. We then present a concrete, assumption-free instance of our algorithm that uses the first and second moments of the empirical inner product distribution only. Furthermore, we make the resulting algorithm space-efficient by designing a sketch [34] of the second moment. The end-result is a practical algorithm that is straightforward to implement.

We put our proposal to the test in Section 3 on a variety of ANN benchmark datasets. As our experiments show, our optimistic router achieves the same ANN recall as state-of-the-art routers but with up to a 50% reduction in the total number of data points evaluated per query. We conclude this work in Section 4.

2 ROUTING BY THE OPTIMISM PRINCIPLE: OUR PROPOSAL

As we observed, NORMALIZEDMEAN is an optimistic estimator, though its behavior is unpredictable. Our goal is to design an optimistic estimator that is statistically principled, thus well-behaved.

Before we begin, let us briefly comment on our terminology and notation. Throughout this section, we fix a unit query vector q ; all discussions are in the context of q . We denote the i -th shard by \mathcal{P}_i , and write S_i for the set of inner product scores between q and points in \mathcal{P}_i : $S_i = \{\langle q, u \rangle : u \in \mathcal{P}_i\}$.

2.1 Formalizing the notion of optimism

We wish to find the *smallest* threshold $\theta_i \geq \langle q, \mu_i \rangle$ for the i -th shard such that the probability that a sample from S_i falls to the left of θ_i is at least $(1 + \delta)/2$, for some arbitrary $\delta \in [0, 1]$. Formally, we aim to compute a solution θ_i to the the following optimization problem:

PROBLEM 1 (OPTIMISTIC ESTIMATOR OF THE MAXIMUM INNER PRODUCT IN S_i).

$$\inf \{\theta_i : \theta_i \geq \langle q, \mu_i \rangle\} \quad \text{such that} \quad \Pr_{s \sim S_i} [s \leq \theta_i] \geq \frac{1 + \delta}{2}.$$

One can interpret the optimal θ_i as a probabilistic upper-bound on the maximum attainable value in S_i ; that is, with some confidence, we can assert that no value in S_i is greater than θ_i .

Equipped with θ_i ’s, we route q by sorting all shards by their estimated thresholds in descending order and selecting the top shards. Our router, dubbed OPTIMIST, is defined as follow:

$$\tau(q) = \arg \max_{i \in [C]}^{(\ell)} \theta_i. \quad (4)$$

2.2 Understanding the routing behavior

Suppose for a moment that we have the solution to Problem 1, and let us expand on the expected behavior of the OPTIMIST router. It is easy to see that, when $\delta \rightarrow 0$, the optimal solution approaches

$\theta_i = \max(\langle q, \mu_i \rangle, \langle q, M_i \rangle)$, where M_i is the median of the i -th partition. That represents the most *conservative* estimate of the maximum inner product between q and points in \mathcal{P}_i .

As $\delta \rightarrow 1$, θ_i becomes larger, rendering Equation (4) an enthusiastically optimistic router. At the extreme, the optimal solution is the maximum inner product itself—the most optimistic we can get.

Clearly then, δ controls the amount of optimism one bestows onto the router. It is interesting to note that, when the data distribution is fully known, then $\delta = 1$ is an appropriate choice: If we know the exact distribution of inner products, we can expect to be fully confident about the maximum inner product. On the other hand, when very little about the distribution is known (e.g., when all we know is the first moment of the distribution), then $\delta = 0$ is a sensible choice. In effect, the value of δ is a statement on our knowledge of the underlying data distribution.

What is left to address is the solution to Problem 1, which is the topic of the remainder of this section. We defer a description of a general approach that uses as much or as little information as available about the data distribution to Appendix A due to space constraints. In the next section, we present a more practical approach that is the foundation of the rest of this work.

2.3 Practical solution via concentration inequalities and sketching

Noting that Problem 1 is captured by the concept of concentration of measure, we resort to results from that literature to find acceptable estimates of θ_i 's. In particular, we obtain a solution via a straightforward application of the one-sided Chebyshev's inequality, resulting in the following lemma.

LEMMA 1. Denote by μ_i and Σ_i the mean and covariance of the distribution of \mathcal{P}_i . An upper-bound on the solution to Problem 1 for $\delta \in (0, 1)$ is:

$$\theta_i = \langle q, \mu_i \rangle + \sqrt{\frac{1+\delta}{1-\delta}} q^\top \Sigma_i q. \quad (5)$$

PROOF. The result follows immediately by applying the one-sided Chebyshev's inequality to the distribution, S_i , of inner products between q and points in \mathcal{P}_i :

$$\begin{aligned} \Pr_{s \sim S_i} [s - \langle q, \mu_i \rangle \leq \epsilon] &\geq 1 - \frac{q^\top \Sigma_i q}{q^\top \Sigma_i q + \epsilon^2} = \frac{1+\delta}{2} \\ \implies \epsilon^2 &= \frac{1+\delta}{1-\delta} q^\top \Sigma_i q. \end{aligned}$$

Rearranging the terms to match the expression of Problem 1 gives $\theta_i = \langle q, \mu_i \rangle + \epsilon$, as desired. \square

We emphasize that the solution obtained by Lemma 1 is not necessarily optimal for Problem 1. Instead, it gives the best upper-bound on the optimal value of θ_i that can be obtained given limited information about the data distribution. As we see later, however, even this sub-optimal solution proves effective in practice.

While Equation (5) gives us an algorithm to approximate the threshold θ_i , storing Σ_i can be prohibitive in practice. That is because the size of the matrix grows as d^2 for each partition. Contrast that with the cost for other routers, such as MEAN and NORMALIZEDMEAN, which only store a single d -dimensional vector per partition (i.e., the mean vector). To remedy this inefficiency, we design a compact approximation of Σ_i that can be plugged into Equation (5) to replace Σ_i . We describe that next to complete our algorithm.

2.3.1 Approximating the covariance matrix. Since the procedure we describe is independently applied to each partition, we drop the subscript in Σ_i and focus on a single partition.

We seek a matrix $\Sigma^* \in \mathbb{R}^{d \times d}$ that approximates the positive semi-definite (PSD) matrix Σ , by minimizing the following standard approximation error:

$$\text{err}(\Sigma, \Sigma^*) \triangleq \sup_{\|v\|_2=1} |v^\top \Sigma v - v^\top \Sigma^* v|. \quad (6)$$

As we seek a *compact* approximation, we constrain the solution space to rank- t matrices: We require $\text{rank}(\Sigma^*) = t$ for some $t \ll d$.

A standard solution to this problem is a result of the Eckhart-Young-Mirsky Theorem: Let $\Sigma = V\Lambda V^\top$ be the eigendecomposition of Σ . Then, $\Sigma^* = [V\sqrt{\Lambda}]_t [V\sqrt{\Lambda}]_t^\top$, where $[\cdot]_t$ is the operator that selects the first t columns of its argument, optimally approximates Σ under the stated constraints. We denote this solution by Σ_t^{LR} .

We could stop here and use Σ_t^{LR} in lieu of Σ in Equation (5). However, while that would be the optimal choice in *the general case*, for real-world datasets, we show that we can find a better approximation. In particular, we present the following:

Definition 1 (Masked Sketch of Rank t). Rewrite Σ as follows, with D containing its diagonal and $R = \Sigma - D$:

$$\Sigma = D + R = D^{\frac{1}{2}} \left(I + \underbrace{D^{-\frac{1}{2}} R D^{-\frac{1}{2}}}_{R_o} \right) D^{\frac{1}{2}}.$$

Let $Q\Lambda Q^\top$ be the eigendecomposition of R_o . We call the following the Masked Sketch of Rank t of Σ :

$$\Sigma_t^{\text{MS}} = D + D^{\frac{1}{2}} [Q]_t [\Lambda]_t [Q]_t^\top D^{\frac{1}{2}}. \quad (7)$$

The following result establishes that, under certain practical assumptions, $\text{err}(\Sigma, \Sigma_t^{\text{MS}})$ can be lower than $\text{err}(\Sigma, \Sigma_t^{\text{LR}})$.

LEMMA 2. *Let $\Sigma \in \mathbb{R}^{d \times d}$ be a PSD matrix with diagonal D for which $\min_{i \in [d]} D_{ii} / \max_{i \in [d]} D_{ii} \geq 1 - \epsilon$ for some $\epsilon > 0$. For every $1 \leq t \leq d - 1$ such that the $(t + 1)$ -th eigenvalue of $D^{-1/2} \Sigma D^{-1/2}$ is greater than 1, we have that: $\text{err}(\Sigma, \Sigma_t^{\text{MS}}) \leq \text{err}(\Sigma, \Sigma_t^{\text{LR}}) \cdot \frac{1}{1 - \epsilon}$.*

We provide a proof for the above result in Appendix B and show that for real-world datasets used in this work, the assumptions in the lemma hold.

2.3.2 The final algorithm. Using our solution from Lemma 1 for Problem 1 and our sketch defined in (7), we describe our full algorithm in Algorithm 1 for building our router and scoring a partition for a given query. Notice that, since we only store $\mu, D, [\Lambda]_t$ and $[Q]_t$, the router requires just $t + 2$ vectors⁵ in \mathbb{R}^d per partition. In our experiments, we choose $t \leq 10$ for all datasets except one and show that much of the performance gains from using the whole covariance matrix can be preserved even by choosing a small value of t independent of d .

3 EXPERIMENTAL EVALUATION

We put our arguments to the test and evaluate OPTIMIST.

3.1 Setup

Datasets: We use the following benchmark datasets in this work:

- **TEXT2IMAGE:** A cross-modal dataset, where data and query points may have different distributions in a shared space [31]. We use a subset consisting of 10 million 200-dimensional data points along with a subset of 10,000 test queries;

⁵Since $[\Lambda]_t$ can be “absorbed” into $[Q]_t$ with some care taken for the signs of the eigenvalues.

Algorithm 1 Indexing and scoring a single partition with OPTIMIST**Input:** Partition \mathcal{P} and target rank $t \ll d$.

```

1: procedure BUILDROUTERFORPARTITION( $\mathcal{P}, t$ )
2:    $\mu \leftarrow \frac{1}{|\mathcal{P}|} \sum_{u \in \mathcal{P}} u$ 
3:    $\Sigma \leftarrow \frac{1}{|\mathcal{P}|} \sum_{u \in \mathcal{P}} (u - \mu)(u - \mu)^\top$ 
4:    $R_o = D^{-1/2}(\Sigma - D)D^{-1/2}$  ▷  $D$  is the diagonal of  $\Sigma$ 
5:   Find eigendecomposition  $R_o = Q\Lambda Q^\top$ 
6:   Sort columns of  $Q, \Lambda$  in non-increasing order
7:    $\Lambda_t \leftarrow [\Lambda]_t, Q_t \leftarrow [Q]_t$ 
8:   return  $\{\mu, D, \Lambda_t, Q_t\}$ 

```

Input: Query $q \in \mathbb{R}^d$ and optimism parameter $\delta > 0$.

```

9: procedure SCOREPARTITIONFORQUERY( $q, \delta; \{\mu, D, \Lambda_t, Q_t\}$ )
10:   $\tilde{q} \leftarrow q \circ \text{diag}(D^{1/2})$  ▷ Element-wise product
11:  return  $\langle q, \mu \rangle + \sqrt{\frac{1+\delta}{1-\delta} \cdot (\|\tilde{q}\|_2^2 + \tilde{q}^\top Q_t \Lambda_t Q_t^\top \tilde{q})}$ 

```

Table 1. Dataset statistics (size m and number of dimensions d), along with the number of partitions (C) and OPTIMIST’s default rank configuration (t) in our main experiments.

DATASET	m	d	C	t
TEXT2IMAGE	10M	200	3,000	4
MUSIC	1M	100	1,024	2
DEEPIIMAGE	10M	96	3,000	2
GLOVE	1.2M	200	1,024	4
MSMARCO-MINILM	8.8M	384	3,000	8
NQ-ADA2	2.7M	1,536	1,600	30

- **MUSIC**: 1 million 100-dimensional points [26] with 1,000 queries;
- **DEEPIIMAGE**: Subset of 10 million 96-dimensional points from the billion deep image features dataset [36] with 10,000 queries;
- **GLOVE**: 1.2 million, 200-dimensional word embeddings trained on tweets [30] with 10,000 test queries;
- **MSMARCO-MINILM**: Ms MARCO Passage Retrieval v1 [27] is a question-answering dataset consisting of 8.8 million short passages in English. We use the “dev” set of queries for retrieval, made up of 6,980 questions. We embed individual passages and queries using the ALL-MINILM-L6-v2 model⁶ to form a 384-dimensional vector collection; and,
- **NQ-ADA2**: 2.7 million, 1,536-dimensional embeddings of the Natural Questions dataset [23] with the ADA-002 model.⁷

We note that the last four datasets are intended for cosine similarity search. As such we normalize these collections prior to indexing, reducing the task to MIPS of Equation (1).

Clustering: For our main results, we partition datasets with Spherical KMeans [12]. We include in the appendix results from similar experiments but where the clustering algorithm is standard

⁶Checkpoint at <https://huggingface.co/sentence-transformers/all-MiniLM-L6-v2>.

⁷<https://openai.com/index/new-and-improved-embedding-model/>

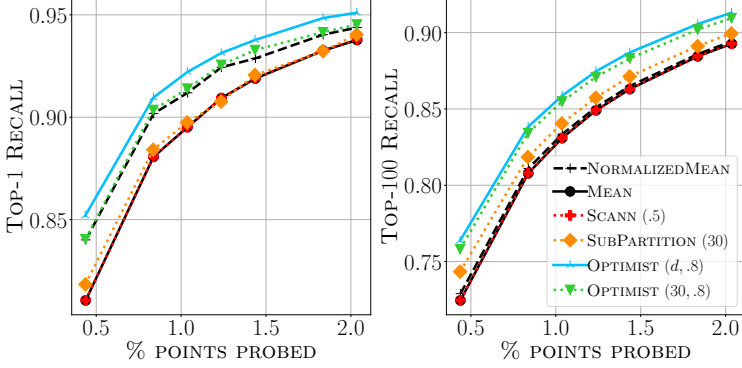


Fig. 2. Top- k recall on NQ-ADA2 vs. volume of probed data points. Setup is as Figure 3.

KMeans and Gaussian Mixture Model (GMM). We cluster each dataset into \sqrt{m} shards, where m is the number of data points in the dataset; this is summarized in Table 1.

Evaluation: Once a dataset has been partitioned, we fix the partitioning and evaluate all routers on it to facilitate a fair comparison. We evaluate each router τ as follows. For each test query, we identify the set of shards to probe using τ . We then perform exact search over the selected shards, obtain the top- k points, and compute recall with respect to the ground-truth top- k set. Because the only source of error is the router’s inaccuracy, the measured recall gauges the effectiveness of τ .

We report recall as a function of the number of *data points* probed, rather than the number of *shards probed*. In this way, a comparison of the efficacy of different routers is unaffected by any imbalance in shard sizes, so that a router cannot trivially outperform another by simply prioritizing larger shards.

Routers: We evaluate the following routers in our experiments:

- **MEAN** and **NORMALIZEDMEAN**: Defined in Equations (2) and (3);
- **SCANN** (T): Similar to **MEAN** and **NORMALIZEDMEAN**, but where routing is determined by inner product between a query and the SCANN centroids (c.f., Theorem 4.2 in [15]). SCANN has a single hyperparameter T , which we set to 0.5 after tuning;
- **SUBPARTITION** (t): Recall that **OPTIMIST** stores $t + 2$ vectors per partition, where t is the rank in Algorithm 1. We ask if simply partitioning each shard independently into $t + 2$ sub-partitions, and recording the sub-partitions’ centroids as the representatives of that shard attains the same routing accuracy as **OPTIMIST**. At query time, we take the maximum inner product of the query with a shard’s representatives as its score, and sort shards according to this score; and,
- **OPTIMIST** (t, δ): The **OPTIMIST** router given in Algorithm 1. The parameter t determines the rank of the sketch of the covariance matrix, and δ determines the degree of optimism. We set $\delta = 0.8$ and t to a maximum of 2% of d , as summarized in Table 1, but study their effect later. Throughout our discussion, if we do not specify the parameters, it should be understood that **OPTIMIST** is configured with default δ and t . We write **OPTIMIST** ($t = d, \cdot$) to indicate that the full covariance matrix is used.

Code: We have implemented all baseline and proposed routers in the Rust programming language. We have open-sourced⁸ our code along with experimental configuration to facilitate reproducibility.

⁸Available at <https://github.com/Artificial-Memory-Lab/optimist-router>

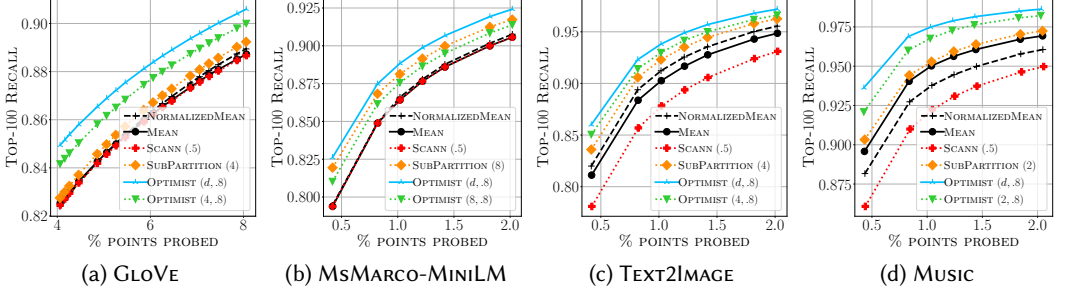


Fig. 3. Top-100 recall vs. volume of probed data. Partitioning is by Spherical KMeans. SCANN has parameter T , SUBPARTITION t (leading to $t + 2$ sub-partitions per shard), and OPTIMIST rank t and degree of optimism δ .

Table 2. Comparison of OPTIMIST and NORMALIZEDMEAN by relative amount of data points saved during search to achieve a fixed recall. A saving of $x\%$ means that OPTIMIST searches $x\%$ fewer points than NORMALIZEDMEAN.

RECALL	NQ-ADA2	GloVe	MsMARCO-MINI LM	MUSIC	TEXT2IMAGE
90%	18%	11%	22%	38%	23%
95%	20%	5.5%	7.7%	54%	22%

3.2 Main results

Figure 2 plots top- k recall for $k \in \{1, 100\}$, versus the percentage of data points examined for NQ-ADA2—see Figure 9 in Appendix C for other datasets and $k \in \{1, 10, 100\}$. Partitioning is by Spherical KMeans; for standard KMeans and GMM see Figures 10 and 11.

We summarize key observations. First, among baselines, NORMALIZEDMEAN generally outperforms MEAN and SCANN, except MUSIC where MEAN reaches a higher recall. Second, with very few exceptions, OPTIMIST with the full covariance ($t = d$) does at least as well as NORMALIZEDMEAN, and often outperforms it significantly. Interestingly, the gap between baselines and OPTIMIST widens as retrieval depth (k) increases; a phenomenon that is not surprising.

Finally, while OPTIMIST with a rank- t Masked Sketch shows some degradation in comparison with no sketching (i.e., $t = d$), it still achieves a higher recall than baselines for larger k . When k is smaller, SUBPARTITION (t) becomes a strong competitor.

OPTIMIST shines when data points have varying norms. This is illustrated in Figure 3, showing top-100 recall on select datasets—refer to Figure 9 for full results. On MUSIC, at 95% top-100 recall, OPTIMIST needs to probe 54% fewer data points than NORMALIZEDMEAN; on average OPTIMIST probes 6,666 data points to reach 95% top-100 recall whereas NORMALIZEDMEAN examines 14,463 points.

Table 2 presents savings on all datasets. On DEEPIIMAGE, OPTIMIST scans 9% *more* data points than NORMALIZEDMEAN to reach 90% recall (55,000 points vs 60,000), and 10% more to reach 95% (95,000 vs 105,000). We suspect this is an artifact of the dataset’s construction: each point is represented by the top 96 principal components of its original features, leading to unusual partition statistics.

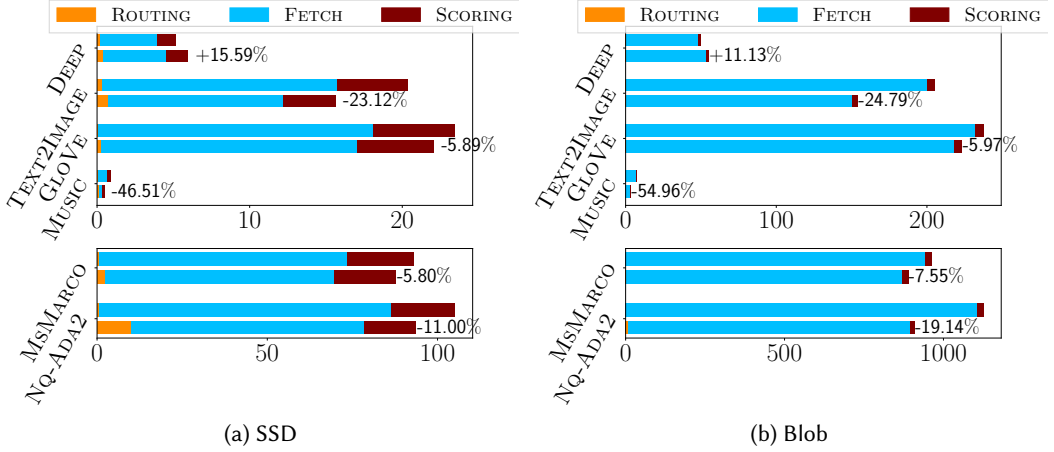


Fig. 4. Mean per-query latency (milliseconds) to reach 95% recall, with 4 threads. For each dataset, we plot the latency breakdown for NORMALIZEDMEAN (top bar) and OPTIMIST (bottom bar), and report relative gains (negative indicates improvements) achieved by OPTIMIST with respect to NORMALIZEDMEAN. Shards are stored as PQ-compressed sets using 4-dimensional codebooks—a common configuration.

3.2.1 Latency. As Table 2 shows, OPTIMIST reaches 95% recall by processing up to 54% fewer points. We now study the impact of the improved routing accuracy on query latency, which consists of routing, fetching the chosen shards from storage, and scoring.

Concretely, we isolate routing and measure the elapsed time between when a router receives a query and when it returns a list of shards. This is the “routing” latency. We then measure the time it takes to fetch the chosen shards from storage; the “fetch” latency. Finally, we measure the latency of the scoring phase. We note that, for latency experiments only, we compress data points and compute inner products using PQ with 4-dimensional codebooks.

We run experiments on an AWS c5.xlarge machine with 4 vCPUs, 8GB of main memory. Baseline bandwidth of the SSD attached to this machine is 1,150Mbps.⁹ Finally, using 4 threads, transferring 4MB of data from blob storage (hosted on Amazon S3) to main memory has P50 latency of 45 milliseconds (ms).¹⁰

Figure 4 reports the routing, fetch, and scoring latency for OPTIMIST and NORMALIZEDMEAN routers, when using 4 threads; we have included results for 1 and 2 threads in Figure 12. As the figure shows, OPTIMIST’s gains are more pronounced when shards are stored on blob storage, but even on SSD the gains are substantial.

We note that, hardware plays an outsize role in latency improvements. Depending on the specifications, we may have a slower or faster interface with blob or SSD storage; a more limited bandwidth would boost OPTIMIST’s standing in latency comparisons. On the other hand, if storage bandwidth is abundant and number of threads very limited, OPTIMIST’s advantage would become less significant.

There are other factors that may affect the overall latency comparison. These include: target recall level; type of compression; and algorithm used for scoring. In the above experiments, we put OPTIMIST at a disadvantage by incorporating heavy compression and fast score computation;

⁹See official benchmark from Amazon at <https://docs.aws.amazon.com/AWSEC2/latest/UserGuide/ebs-optimized.html>

¹⁰See <https://github.com/dvassallo/s3-benchmark> for an independent benchmark.

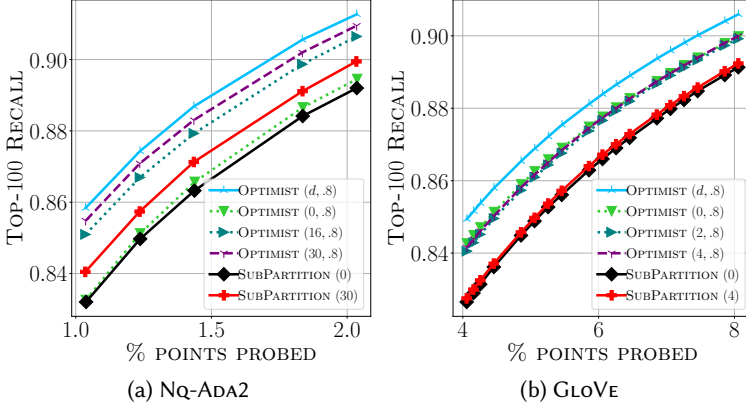


Fig. 5. Top-100 recall vs. volume of probed data, comparing a range of values for the rank of the covariance sketch (t), with SUBPARTITION(t). OPTIMIST($0, \cdot$) denotes a sketch that only retains the diagonals.

OPTIMIST fares even better if data remains uncompressed (as OPTIMIST needs to transfer a smaller amount of data) or scoring is slower (as OPTIMIST must score fewer points).

3.2.2 Router size. As we noted, a router such as NORMALIZEDMEAN that uses a point estimate to score shards needs to store only a single d -dimensional vector per shard. OPTIMIST, on the other hand, requires $(t + 2)$ vectors in \mathbb{R}^d per shard to make its routing decision. Here, we present concrete numbers for completeness, and compare the size of the two routers on the datasets used in our experiments.

On most datasets, the difference in size between NORMALIZEDMEAN and OPTIMIST is negligible. On GloVe, for example, NORMALIZEDMEAN takes up 0.8MB of space while OPTIMIST ($t = 4$) consumes 4.7MB in total. Statistics on other datasets are as follows: on MsMARCO-MINI LM it is 4.4MB for NORMALIZEDMEAN versus 44MB for OPTIMIST ($t = 8$); on MUSIC, 0.4MB versus 1.6MB ($t = 2$); on TEXT2IMAGE, 2.3MB versus 13.7MB ($t = 4$); on DEEPIMAGE, 1.1MB versus 4.4MB ($t = 2$). The difference is larger, but still mild, on NQ-ADA2: 9.4MB versus 300MB ($t = 30$).

3.3 Effect of parameters on OPTIMIST

Recall that OPTIMIST takes two parameters: t , the rank of the covariance sketch, and δ , the degree of optimism. We examine the effect of these parameters on the performance of OPTIMIST.

Figure 5 visualizes the role played by t for a subset of datasets—with the remaining figures included in Figure 13 in Appendix C. It comes as no surprise that larger values of t lead to a better approximation of the covariance matrix. What we found interesting, however, is the remarkable effectiveness of a sketch that simply retains the diagonal of the covariance, denoted by OPTIMIST($0, \cdot$), in the settings of k we experimented with (i.e., $k \in \{1, 10, 100\}$).

In the same figure, we have also included two configurations of SUBPARTITION: one with 2 sub-partitions, SUBPARTITION(0), and another with $t + 2$ sub-partitions, SUBPARTITION(t), for the largest t . These help put the performance of OPTIMIST with various ranks in perspective. In particular, we give the SUBPARTITION baseline the same amount of information and contrast its recall with OPTIMIST.

We turn to Figure 6 to understand the impact of δ —we refer the reader to Figure 14 in Appendix C for analysis on the remaining datasets. It is clear that encouraging OPTIMIST to be too optimistic

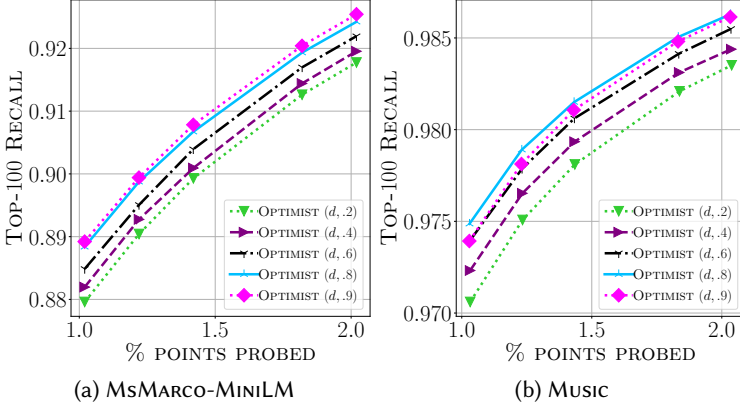


Fig. 6. Recall vs. volume of probed data for different values of δ . As $\delta \rightarrow 1$, OPTIMIST becomes more optimistic.

can lead to sub-optimal performance. That is because of our reliance on the Chebyshev’s inequality, which can prove too loose, leading to an overestimation of the maximum value. Interestingly, $\delta \in (0.6, 0.8)$ appears to yield better recall across datasets.

3.4 Maximum inner product prediction

We claimed that OPTIMIST is statistically principled. We expect then, that it should give more accurate estimates of the maximum inner product for any given query-partition pair. We examine that claim in this section and quantify the prediction error for all routers.

Fix a dataset, whose C partitions are denoted by \mathcal{P}_i for $i \in [C]$, along with a router τ and query q . We write τ_i to denote the score computed by τ for partition \mathcal{P}_i and q ; for example, NORMALIZEDMEAN computes $\langle q, \mu_i / \|\mu_i\|_2 \rangle$ and OPTIMIST θ_i per Equation (5).

Note that, the τ_i ’s induce an ordering among partitions. We denote this permutation by π , so that $\tau_{\pi_i} \geq \tau_{\pi_{i+1}}$. We quantify the prediction error for $\ell \in [C]$ as:

$$\mathcal{E}_\ell(\tau, q) = \frac{1}{\ell} \sum_{i=1}^{\ell} \left| \frac{\tau_{\pi_i}}{\max_{u \in \mathcal{P}_{\pi_i}} \langle q, u \rangle} - 1 \right|. \quad (8)$$

This error is 0 when scores produced by the router perfectly match the maximum inner product. The role of ℓ is to allow us to factor in the rank of partitions in our characterization of the prediction error. In other words, we can measure the error only for the top ℓ shards according to τ . In this way, if we decide that it is not imperative for a router to accurately predict the maximum inner product in low-ranking shards, we can reflect that choice in our calculation.

We measure Equation (8) on all datasets partitioned by Spherical KMeans, and all routers considered in this work. The results are shown in Figure 7, where for each choice of ℓ , we plot $\mathbb{E}_q[\mathcal{E}_\ell(\tau, q)]$ for test queries.

From the figures, with the exception of SCANN on TEXT2IMAGE, it is clear that all routers suffer a greater error as $\ell \rightarrow C$ (i.e., % shards approaches 100%). Interestingly, OPTIMIST($t = d, \cdot$) degrades much less severely. Remarkably, when $t \ll d$, the same pattern persists; MUSIC excepted, where, with $t = 2$, OPTIMIST becomes highly inaccurate when $\ell \geq 8\%$ of the total number of shards.

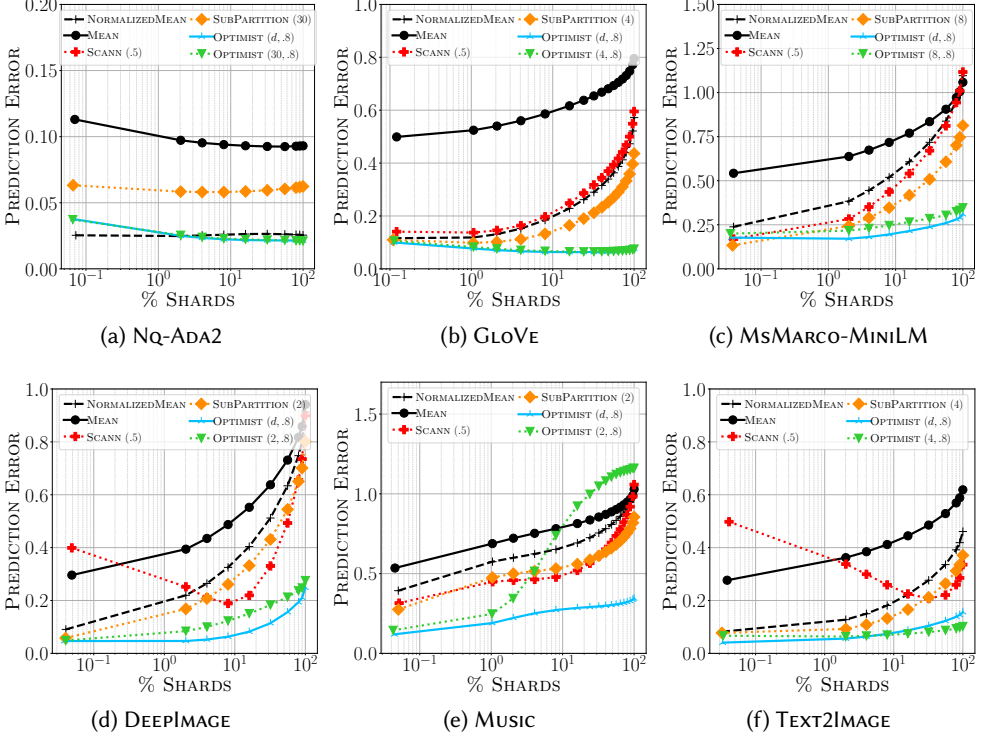


Fig. 7. Mean prediction error $\mathcal{E}_\ell(\tau, \cdot)$, defined in Equation (8), versus ℓ (expressed as percent of total number of shards), for various routers and datasets.

4 CONCLUDING REMARKS

We studied clustering-based maximum inner product search, where data points are clustered into non-overlapping shards to form an index. At query time, two independent components work together to process a query: a *router* computes a score for each shard with respect to the query and identifies the subset of top shards to probe; and a subsequent *scoring* stage that computes (approximate) scores for points in the chosen shards. In this general setup, we considered a storage-backed system where shards do not rest in the main memory, but are stored on external storage and must be fetched into the main memory when a router identifies them. This is an important paradigm for vector search at scale.

Within this framework, we focused on routing. We motivated our work by an unusual but unsurprising observation: NORMALIZEDMEAN computes a score for each shard that over-estimates the maximum inner product between an arbitrary query and the points in that shard. Interestingly, the extent of over-estimation correlates with the variance of the shard: The more spread-out the points are, the more optimistic the NORMALIZEDMEAN router becomes.

This behavior is unpredictable, however. It is also hard to explain why it leads to more accurate routing when data points have non-constant norms. But we found the insight that variance should play a role in routing to be worth investigating. We formalized that insight and presented a principled

optimistic algorithm whose score for a shard is a more accurate estimate of the maximum inner product—as confirmed by evidence in Figure 7.

As Figure 4 shows, our algorithm, OPTIMIST, is more suitable for settings where shards rest on some external, high-latency storage. That is because, in such settings, spending more computation on routing is acceptable if we end up transferring a smaller amount of data from storage to main memory. It is particularly attractive when the storage medium is a cheap, high-latency blob storage.

OPTIMIST has other implications beyond latency. Needing to transfer a smaller volume of data to memory means that each query requires a smaller chunk of the in-memory cache. As a result, cache can be shared among more queries, leading to a higher throughput in systems where memory availability is the main bottleneck.

Our research takes a first step in exploring unsupervised routing for clustering-based MIPS, and identifies a trade-off space that has not been explored previously. We have more to do, however. We leave to future work an exploration of a more compact sketch of the covariance matrix; and, an efficient realization of our general solution outlined in Appendix A.

REFERENCES

- [1] Nir Ailon and Bernard Chazelle. 2009. The fast Johnson–Lindenstrauss transform and approximate nearest neighbors. *SIAM Journal on computing* 39, 1 (2009), 302–322.
- [2] Nir Ailon and Edo Liberty. 2013. An almost optimal unrestricted fast Johnson-Lindenstrauss transform. *ACM Transactions on Algorithms (TALG)* 9, 3 (2013), 1–12.
- [3] Fabien Andre, Anne-Marie Kermarrec, and Nicolas Le Scouarnec. 2021. Quicker ADC: Unlocking the Hidden Potential of Product Quantization With SIMD. *IEEE Transactions on Pattern Analysis and Machine Intelligence* 43, 5 (5 2021), 1666–1677.
- [4] Alex Auvolat, Sarath Chandar, Pascal Vincent, Hugo Larochelle, and Yoshua Bengio. 2015. Clustering is Efficient for Approximate Maximum Inner Product Search. arXiv:1507.05910 [cs.LG]
- [5] Artem Babenko and Victor Lempitsky. 2012. The inverted multi-index. In *2012 IEEE Conference on Computer Vision and Pattern Recognition*. 3069–3076.
- [6] Jon Louis Bentley. 1975. Multidimensional Binary Search Trees Used for Associative Searching. *Commun. ACM* 18, 9 (9 1975), 509–517.
- [7] Vladimir Braverman, Aditya Krishnan, and Christopher Musco. 2022. Sublinear time spectral density estimation. In *Proceedings of the 54th Annual ACM SIGACT Symposium on Theory of Computing*. 1144–1157.
- [8] Sebastian Bruch. 2024. *Foundations of Vector Retrieval*. Springer Nature Switzerland.
- [9] Sebastian Bruch, Franco Maria Nardini, Amir Ingber, and Edo Liberty. 2024. Bridging Dense and Sparse Maximum Inner Product Search. *ACM Transactions on Information Systems* 42, 6 (Aug. 2024), 1–38.
- [10] Flavio Chierichetti, Alessandro Panconesi, Prabhakar Raghavan, Mauro Sozio, Alessandro Tiberi, and Eli Upfal. 2007. Finding near Neighbors through Cluster Pruning. In *Proceedings of the 26th ACM SIGMOD-SIGACT-SIGART Symposium on Principles of Database Systems* (Beijing, China). 103–112.
- [11] Sanjoy Dasgupta and Kaushik Sinha. 2015. Randomized Partition Trees for Nearest Neighbor Search. *Algorithmica* 72, 1 (5 2015), 237–263.
- [12] Inderjit S. Dhillon and Dharmendra S. Modha. 2001. Concept Decompositions for Large Sparse Text Data Using Clustering. *Machine Learning* 42, 1 (January 2001), 143–175.
- [13] Matthijs Douze, Alexandr Guzhva, Chengqi Deng, Jeff Johnson, Gergely Szilvasy, Pierre-Emmanuel Mazaré, Maria Lomeli, Lucas Hosseini, and Hervé Jégou. 2024. The Faiss library. arXiv:2401.08281 [cs.LG]
- [14] Tiezheng Ge, Kaiming He, Qifa Ke, and Jian Sun. 2014. Optimized Product Quantization. *IEEE Transactions on Pattern Analysis and Machine Intelligence* 36, 4 (2014), 744–755.
- [15] Ruiqi Guo, Philip Sun, Erik Lindgren, Quan Geng, David Simcha, Felix Chern, and Sanjiv Kumar. 2020. Accelerating large-scale inference with anisotropic vector quantization. In *Proceedings of the 37th International Conference on Machine Learning*. Article 364, 10 pages.
- [16] Piotr Indyk and Rajeev Motwani. 1998. Approximate Nearest Neighbors: Towards Removing the Curse of Dimensionality. In *Proceedings of the 30th Annual ACM Symposium on Theory of Computing* (Dallas, Texas, USA). 604–613.
- [17] Shikhar Jaiswal, Ravishankar Krishnaswamy, Ankit Garg, Harsha Vardhan Simhadri, and Sheshansh Agrawal. 2022. OOD-DiskANN: Efficient and Scalable Graph ANNS for Out-of-Distribution Queries. arXiv:2211.12850 [cs.LG]
- [18] Suhas Jayaram Subramanya, Fnu Devvrit, Harsha Vardhan Simhadri, Ravishankar Krishnaswamy, and Rohan Kadekodi. 2019. DiskANN: Fast Accurate Billion-point Nearest Neighbor Search on a Single Node. In *Advances in Neural*

Information Processing Systems, Vol. 32.

- [19] Herve Jégou, Matthijs Douze, and Cordelia Schmid. 2011. Product Quantization for Nearest Neighbor Search. *IEEE Transactions on Pattern Analysis and Machine Intelligence* 33, 1 (2011), 117–128.
- [20] Jeff Johnson, Matthijs Douze, and Hervé Jégou. 2021. Billion-Scale Similarity Search with GPUs. *IEEE Transactions on Big Data* 7, 3 (2021), 535–547.
- [21] Yannis Kalantidis and Yannis Avrithis. 2014. Locally Optimized Product Quantization for Approximate Nearest Neighbor Search. In *2014 IEEE Conference on Computer Vision and Pattern Recognition*. 2329–2336.
- [22] Weihao Kong and Gregory Valiant. 2017. Spectrum Estimation from Samples. *The Annals of Statistics* 45, 5 (2017), 2218–2247.
- [23] Tom Kwiatkowski, Jennimaria Palomaki, Olivia Redfield, Michael Collins, Ankur Parikh, Chris Alberti, Danielle Epstein, Illia Polosukhin, Jacob Devlin, Kenton Lee, Kristina Toutanova, Llion Jones, Matthew Kelcey, Ming-Wei Chang, Andrew M. Dai, Jakob Uszkoreit, Quoc Le, and Slav Petrov. 2019. Natural Questions: A Benchmark for Question Answering Research. *Transactions of the Association for Computational Linguistics* 7 (2019), 452–466.
- [24] Tor Lattimore and Csaba Szepesvári. 2020. *Bandit algorithms*. Cambridge University Press.
- [25] Yu A. Malkov and D. A. Yashunin. 2020. Efficient and Robust Approximate Nearest Neighbor Search Using Hierarchical Navigable Small World Graphs. *IEEE Transactions on Pattern Analysis and Machine Intelligence* 42, 4 (4 2020), 824–836.
- [26] Stanislav Morozov and Artem Babenko. 2018. Non-metric Similarity Graphs for Maximum Inner Product Search. In *Advances in Neural Information Processing Systems*, Vol. 31. Curran Associates, Inc.
- [27] Tri Nguyen, Mir Rosenberg, Xia Song, Jianfeng Gao, Saurabh Tiwary, Rangan Majumder, and Li Deng. 2016. MS MARCO: A Human Generated MACHine Reading Comprehension Dataset.
- [28] Mohammad Norouzi and David J. Fleet. 2013. Cartesian K-Means. In *Proceedings of the 2013 IEEE Conference on Computer Vision and Pattern Recognition*. 3017–3024.
- [29] Karl Pearson. 1936. Method of moments and method of maximum likelihood. *Biometrika* 28, 1/2 (1936), 34–59.
- [30] Jeffrey Pennington, Richard Socher, and Christopher Manning. 2014. GloVe: Global Vectors for Word Representation. In *Proceedings of the 2014 Conference on Empirical Methods in Natural Language Processing*. Doha, Qatar, 1532–1543.
- [31] Harsha Vardhan Simhadri, George Williams, Martin Aumüller, Matthijs Douze, Artem Babenko, Dmitry Baranchuk, Qi Chen, Lucas Hosseini, Ravishankar Krishnaswamy, Gopal Srinivasa, Suhas Jayaram Subramanya, and Jingdong Wang. 2022. Results of the NeurIPS’21 Challenge on Billion-Scale Approximate Nearest Neighbor Search. In *Proceedings of the NeurIPS 2021 Competitions and Demonstrations Track (Proceedings of Machine Learning Research, Vol. 176)*. 177–189.
- [32] Aditi Singh, Suhas Jayaram Subramanya, Ravishankar Krishnaswamy, and Harsha Vardhan Simhadri. 2021. FreshDiskANN: A Fast and Accurate Graph-Based ANN Index for Streaming Similarity Search. arXiv:2105.09613 [cs.IR]
- [33] Thomas Vecchiato, Claudio Lucchese, Franco Maria Nardini, and Sebastian Bruch. 2024. A Learning-to-Rank Formulation of Clustering-Based Approximate Nearest Neighbor Search. In *Proceedings of the 47th International ACM SIGIR Conference on Research and Development in Information Retrieval*. (to appear).
- [34] David P. Woodruff. 2014. Sketching as a Tool for Numerical Linear Algebra. *Foundations and Trends in Theoretical Computer Science* 10, 1–2 (Oct 2014), 1–157.
- [35] Xiang Wu, Ruiqi Guo, Ananda Theertha Suresh, Sanjiv Kumar, Daniel N Holtmann-Rice, David Simcha, and Felix Yu. 2017. Multiscale Quantization for Fast Similarity Search. In *Advances in Neural Information Processing Systems*, Vol. 30.
- [36] Artem Babenko Yandex and Victor Lempitsky. 2016. Efficient Indexing of Billion-Scale Datasets of Deep Descriptors. In *2016 IEEE Conference on Computer Vision and Pattern Recognition*. 2055–2063.

A GENERAL SOLUTION

Let \mathcal{D} be an unknown distribution over \mathbb{R}^d from which shard \mathcal{P}_i is sampled. It is clear that, if we are able to accurately approximate the quantiles of S_i , we can obtain an estimate θ_i satisfying Problem 1.

Let us motivate our approach by considering a special case where \mathcal{D} is $\mathcal{N}(\mu_i, \Sigma_i)$, a Gaussian with mean $\mu_i \in \mathbb{R}^d$ and covariance $\Sigma_i \in \mathbb{R}^{d \times d}$. In this case, S_i follows a univariate Gaussian distribution with mean $\langle q, \mu_i \rangle$ and variance $q^\top \Sigma_i q$. In this setup, a solution to Problem 1 is simply:

$$\theta_i = \langle q, \mu_i \rangle + \sqrt{q^\top \Sigma_i q} \cdot \Phi_{\mathcal{N}(0,1)}^{-1} \left(\frac{1 + \delta}{2} \right), \quad (9)$$

which follows by expressing the cumulative distribution function (CDF) of S_i in terms of the CDF of a unit Gaussian, denoted by $\Phi_{\mathcal{N}(0,1)}$.

Notice in the above example that, we first modeled the moments of S_i using the moments of \mathcal{D} . We then approximated the CDF (or equivalently, the quantile function) of the distribution of S_i using its moments—in the Gaussian case, the approximation with the first two moments is, in fact, exact.

Our general solution follows that same logic. In the first step, we can obtain the first r moments of the distribution of S_i , denoted by $m_j(S_i)$ for $j \in [r]$, from the moments of \mathcal{D} , denoted by $m_j(\mathcal{D})$. In a subsequent step, we use $m_j(S_i)$'s to approximate the CDF of S_i .

It is easy to see that the j -th moment of S_i can be written as follows:

$$m_j(S_i) = q^{\otimes j} \odot m_j(\mathcal{D}) \approx \frac{1}{n} \cdot q^{\otimes j} \odot \sum_{u_1, \dots, u_n \sim \mathcal{D}} x^{\otimes j},$$

where $^{\otimes j}$ is the j -fold tensor product, and \odot tensor inner product.

In our second step, we wish to find a distribution \tilde{S}_i such that $m_j(\tilde{S}_i) \approx m_j(S_i)$ for all $j \in [r]$. This can be done using the “method of moments,” a classic technique in statistics [29] that offers guarantees [7, 22] in terms of a distributional distance such as the Wasserstein-1 distance.

While using higher-order moments can lead to a better approximation, computing the j -th moment for $j > 2$ can be highly expensive considering the dimensionality of datasets seen in practice, as the memory requirement to store the tensor $m_j(\mathcal{D})$ grows as d^j . We leave exploration and design of an efficient version of this two-step approach as future work.

B SKETCHING THE COVARIANCE MATRIX

Let $\Sigma = D + R$ be the decomposition of the PSD covariance matrix Σ into its diagonal D and residual $R = \Sigma - D$. Let $Q\Lambda Q^\top$ be the orthogonal eigendecomposition of $R_o = D^{-1/2}RD^{-1/2}$. Recall that we define Σ_t^{MS} , for some $1 \leq t \leq d$, as

$$\Sigma_t^{\text{MS}} := D + D^{1/2}[Q]_t[\Lambda]_t[Q]_t^\top D^{1/2}$$

We start by proving Lemma 2. We then proceed to justify the assumptions of the lemma in the subsequent section.

B.1 Proof of Lemma 2

Let us first state a few technical lemmas that will simplify our proof of Lemma 2.

FACT 1. *For any symmetric matrix $M \in \mathbb{R}^{d \times d}$ with eigendecomposition USU^\top , we have that for any $v \in \mathbb{R}^d$,*

$$v^\top M v = \sum_{i=1}^d S_i \cdot \langle v, U_i \rangle^2.$$

FACT 2. Assuming the eigenvalues Λ of R_o are sorted in non-increasing order, we have that $I + R_o = Q(I + \Lambda)Q^\top$. In words, the eigenvectors of $I + R_o$ are the same as R_o , and the i -th eigenvalue is $\Lambda_i + 1$. As a corollary, since $I + R_o$ is PSD, we have that $\Lambda_i \geq -1$ for all $i \in [d]$.

PROOF. This follows easily after noticing that $I = QQ^\top$ because Q is a $d \times d$ matrix with orthonormal columns (and rows). \square

FACT 3. For a diagonal matrix $S \in \mathbb{R}^{d \times d}$ with bounded positive entries, i.e. $0 < l \leq S_{ii} \leq u$ for all $i \in [d]$, and arbitrary vector $v \in \mathbb{R}^d$, we have that $l\|v\|_2 \leq \|Sv\|_2 \leq u\|v\|_2$.

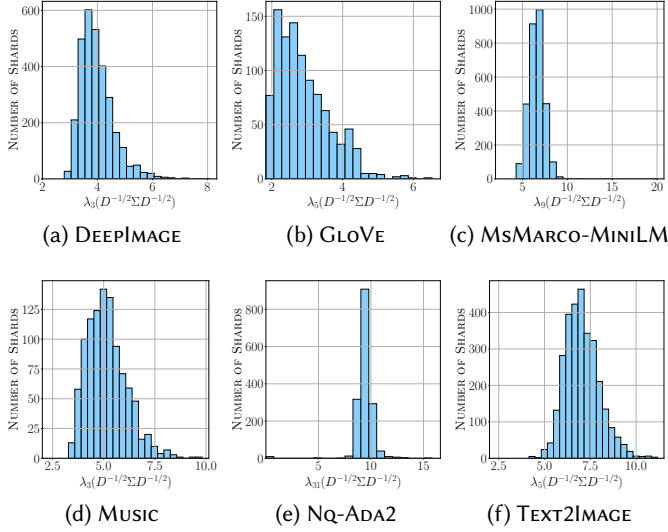


Fig. 8. Histogram of the $(t + 1)$ -th eigenvalue. For each dataset, we pick the partitioning and t from Table 1. Plots show that almost all shards for all datasets have $(t + 1)$ -th eigenvalue bounded away from 1, except for a few shards for NQ-ADA2.

PROOF OF LEMMA 2. First, note that, by the definition of $\text{err}(\cdot, \cdot)$ from Equation (6), we can write:

$$\text{err}(D^{-\frac{1}{2}}\Sigma D^{-\frac{1}{2}}, D^{-\frac{1}{2}}\Sigma_t^{\text{MS}} D^{-\frac{1}{2}}) = \sup_{v \in \mathbb{R}^d} \frac{|v^\top D^{-1/2}(\Sigma - \Sigma_t^{\text{MS}})D^{-1/2}v|}{\|v\|_2^2}.$$

Since D has strictly positive entries on the diagonal, we can do a change of variables, setting $u = D^{1/2}v$. Denoting $\max_{i \in [d]} D_{ii}$ by $\|D\|_\infty$, this gives us:

$$\begin{aligned} \text{err}(D^{-\frac{1}{2}}\Sigma D^{-\frac{1}{2}}, D^{-\frac{1}{2}}\Sigma_t^{\text{MS}} D^{-\frac{1}{2}}) &= \sup_{v \in \mathbb{R}^d} \frac{|v^\top (\Sigma - \Sigma_t^{\text{MS}})v|}{\|D^{1/2}v\|_2^2} \\ &\geq \frac{1}{\|D\|_\infty} \cdot \sup_{v \in \mathbb{R}^d} \frac{|v^\top (\Sigma - \Sigma_t^{\text{MS}})v|}{\|v\|_2^2} = \frac{\text{err}(\Sigma, \Sigma_t^{\text{MS}})}{\|D\|_\infty} \end{aligned}$$

where the inequality follows by Fact 3.

Next, consider the following:

$$\begin{aligned} \text{err}(D^{-\frac{1}{2}}\Sigma D^{-\frac{1}{2}}, D^{-\frac{1}{2}}\Sigma_t^{\text{MS}}D^{-\frac{1}{2}}) &= \sup_{\|v\|_2=1} |v^\top D^{-\frac{1}{2}}(\Sigma - \Sigma_t^{\text{MS}})D^{-\frac{1}{2}}v| \\ &= \sup_{\|v\|_2=1} |v^\top (R_o - [Q]_t[\Lambda]_t[Q]_t^\top)v| \end{aligned} \quad (10)$$

$$= \sup_{\|v\|_2=1} \left| \sum_{i=t+1}^d \Lambda_i \cdot \langle Q_i, v \rangle^2 \right| \quad (11)$$

$$= \max_{l \in [t+1, d]} |\Lambda_l|. \quad (12)$$

where the second equality follows by the definition of Σ_t^{MS} and the third by Fact 1.

Putting our arguments thus far together, we have established that:

$$\frac{\text{err}(\Sigma, \Sigma_t^{\text{MS}})}{\|D\|_\infty} \leq \max_{l \in [t+1, d]} |\Lambda_l|. \quad (13)$$

Using this result, and noting that, $1 + \Lambda_{t+1} \geq 1$ by assumption, so that $\Lambda_{t+1} \geq 0$; and $\Lambda_l \geq -1$ for all $l \in [d]$ by Fact 2, we can derive the following:

$$\frac{\text{err}(\Sigma, \Sigma_t^{\text{MS}})}{\|D\|_\infty} \leq \max_{l \in [t+1, d]} |\Lambda_l| \quad (14)$$

$$\leq 1 + \Lambda_{t+1} \quad (15)$$

$$\leq \max_{l \in [t+1, d]} |1 + \Lambda_l| \quad (16)$$

$$= \text{err}(\underbrace{I + R_o}_{D^{-1/2}\Sigma D^{-1/2}}, [Q]_t[I + \Lambda]_t[Q]_t^\top). \quad (17)$$

All that is left to do is to bound the right-hand side of Equation (17). We do so as follows:

$$\text{err}(D^{-1/2}\Sigma D^{-1/2}, [Q]_t[I + \Lambda]_t[Q]_t^\top) \quad (18)$$

$$\leq \text{err}(D^{-1/2}\Sigma D^{-1/2}, D^{-1/2}\Sigma_t^{\text{LR}}D^{-1/2}) \quad (19)$$

$$= \sup_{\|v\|_2=1} |v^\top D^{-1/2}(\Sigma - \Sigma_t^{\text{LR}})D^{-1/2}v| \quad (20)$$

$$= \sup_{\|v\|_2=1} \left| \sum_{i,j} v_i v_j (\Sigma - \Sigma_t^{\text{LR}})_{ij} / \sqrt{D_{ii}D_{jj}} \right| \quad (21)$$

$$\leq \sup_{\|v\|_2=1} \left| \sum_{i,j} v_i v_j (\Sigma - \Sigma_t^{\text{LR}})_{ij} \frac{1}{(1 - \epsilon)\|D\|_\infty} \right| \quad (22)$$

$$\leq \frac{1}{(1 - \epsilon)\|D\|_\infty} \sup_{\|v\|_2=1} |v^\top (\Sigma - \Sigma_t^{\text{LR}})v| \quad (23)$$

$$= \frac{1}{(1 - \epsilon)\|D\|_\infty} \text{err}(\Sigma, \Sigma_t^{\text{LR}}), \quad (24)$$

where the first inequality is because the left-hand side is the optimal error by the Eckhart-Young-Mirsky Theorem, and the second inequality is due to the fact that $D_{ii} \geq (1 - \epsilon)\|D\|_\infty$.

Putting everything together, we have shown that:

$$\frac{\text{err}(\Sigma, \Sigma_t^{\text{MS}})}{\|D\|_\infty} \leq \frac{1}{(1 - \epsilon)\|D\|_\infty} \text{err}(\Sigma, \Sigma_t^{\text{LR}}),$$

as desired. \square

B.2 Assumptions of Lemma 2

Recall that we make two assumptions about the covariance matrix Σ and the eigendecomposition of its symmetrization, $D^{-1/2}\Sigma D^{-1/2}$:

- (1) The $(t + 1)$ -th eigenvalue of $D^{-1/2}\Sigma D^{-1/2}$ is greater than or equal to 1. In particular, letting $D^{-1/2}\Sigma D^{-1/2} = Q(I + \Lambda)Q^\top$ be the orthogonal eigendecomposition of the symmetrization, we assume $1 + \Lambda_{t+1} \geq 1$.
- (2) The diagonal of Σ has the property that $\min_{i \in [d]} \Sigma_{ii} \geq (1 - \epsilon) \max_{i \in [d]} \Sigma_{ii}$ for some $\epsilon \in (0, 1]$.

First assumption. Notice that $D^{-1/2}\Sigma D^{-1/2} = I + D^{-1/2}RD^{-1/2}$ is symmetric PSD, so we have that $\text{tr}(D^{-1/2}\Sigma D^{-1/2}) = \sum_{i=1}^d 1 + \Lambda_i = d$. Hence by definition there must exist some t for which $1 + \Lambda_{t+1} \geq 1$. While in the worst case we cannot hope for the existence of an eigenvalue larger than this, in practice, including for the datasets we consider in this work, it can be shown that in fact the eigenvalues of $D^{-1/2}\Sigma D^{-1/2}$ are larger than 1 across shards and datasets—see Figure 8.

Second assumption. While in the worst case, the diagonal of Σ can have arbitrarily large entries compared to its smallest entries, in practice this is rarely the case. While we do not explore how to remove this assumption, there are several mechanisms to do so in practice such as applying random rotations or pseudo-random rotations [1, 2, 34] to the data points in each shard before using Algorithm 1. It is well known (e.g. Lemma 1 in [1]) that after applying such transforms, the coordinates of the vectors are “roughly equal,” thereby ensuring that the diagonal of the covariance has entries of comparable magnitude. We leave the exploration of removing this assumption to future work.

C ADDITIONAL EXPERIMENTAL RESULTS

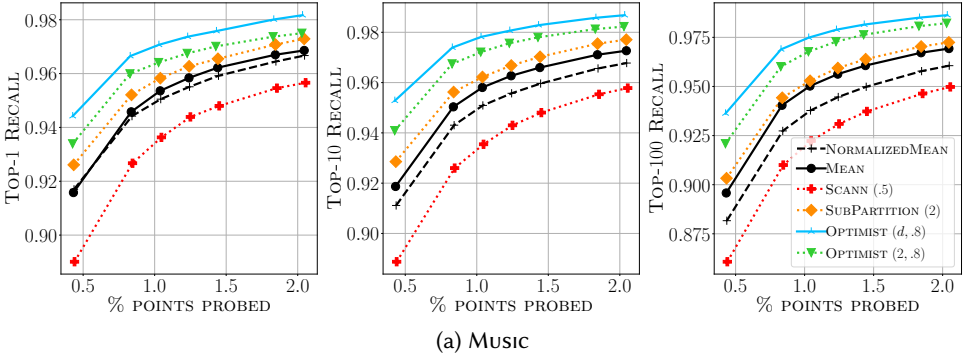


Fig. 9. Top- k recall vs. volume of probed data. Partitioning is with Spherical KMeans. SCANN has parameter T , SUBPARTITION t (leading to $t + 2$ sub-partitions per shard), and OPTIMIST rank t and degree of optimism δ .

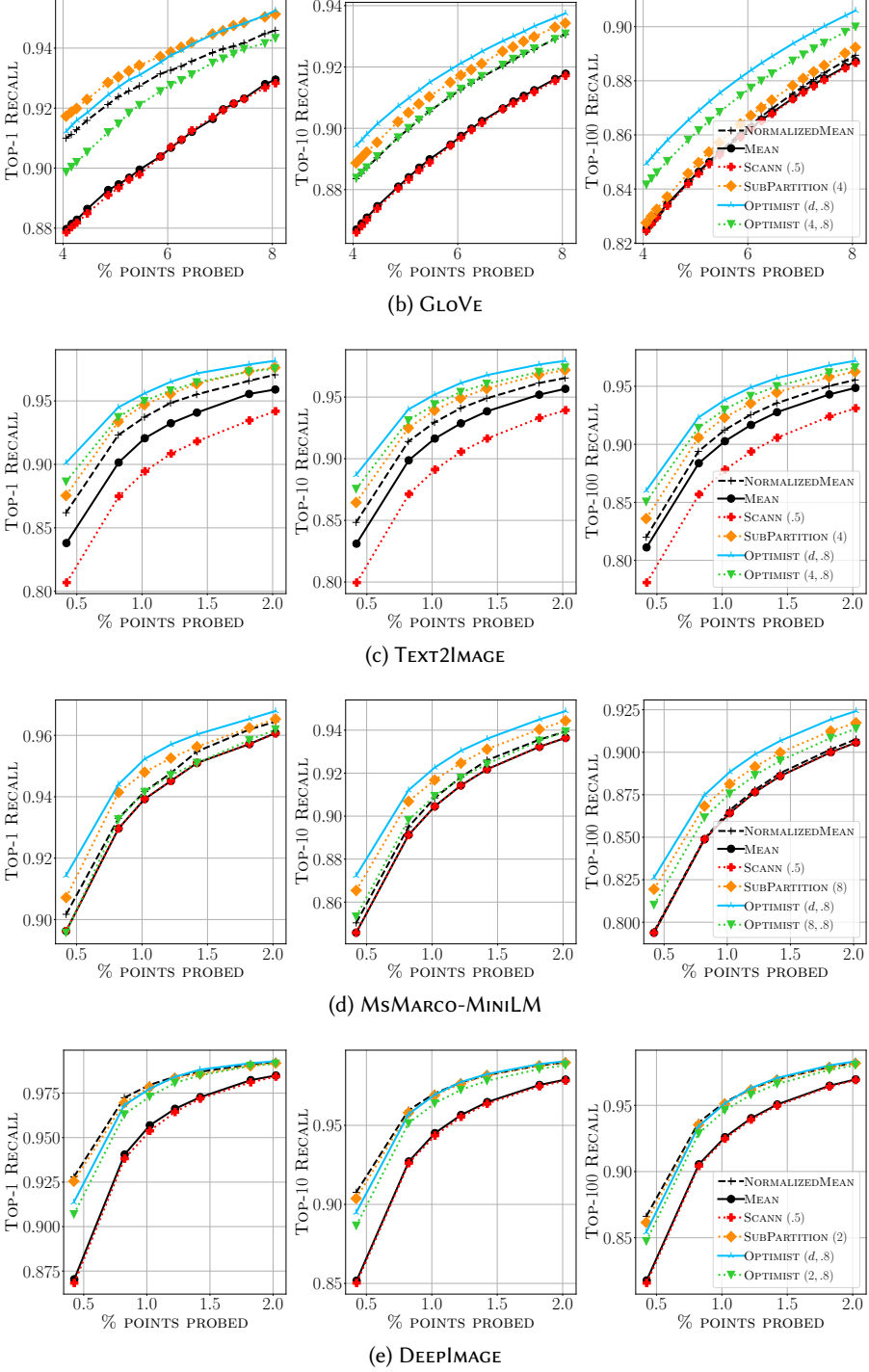


Fig. 9. Top- k recall vs. volume of probed data. Partitioning is with Spherical KMeans. SCANN has parameter T , SUBPARTITION t (leading to $t + 2$ sub-partitions per shard), and OPTIMIST rank t and degree of optimism δ .

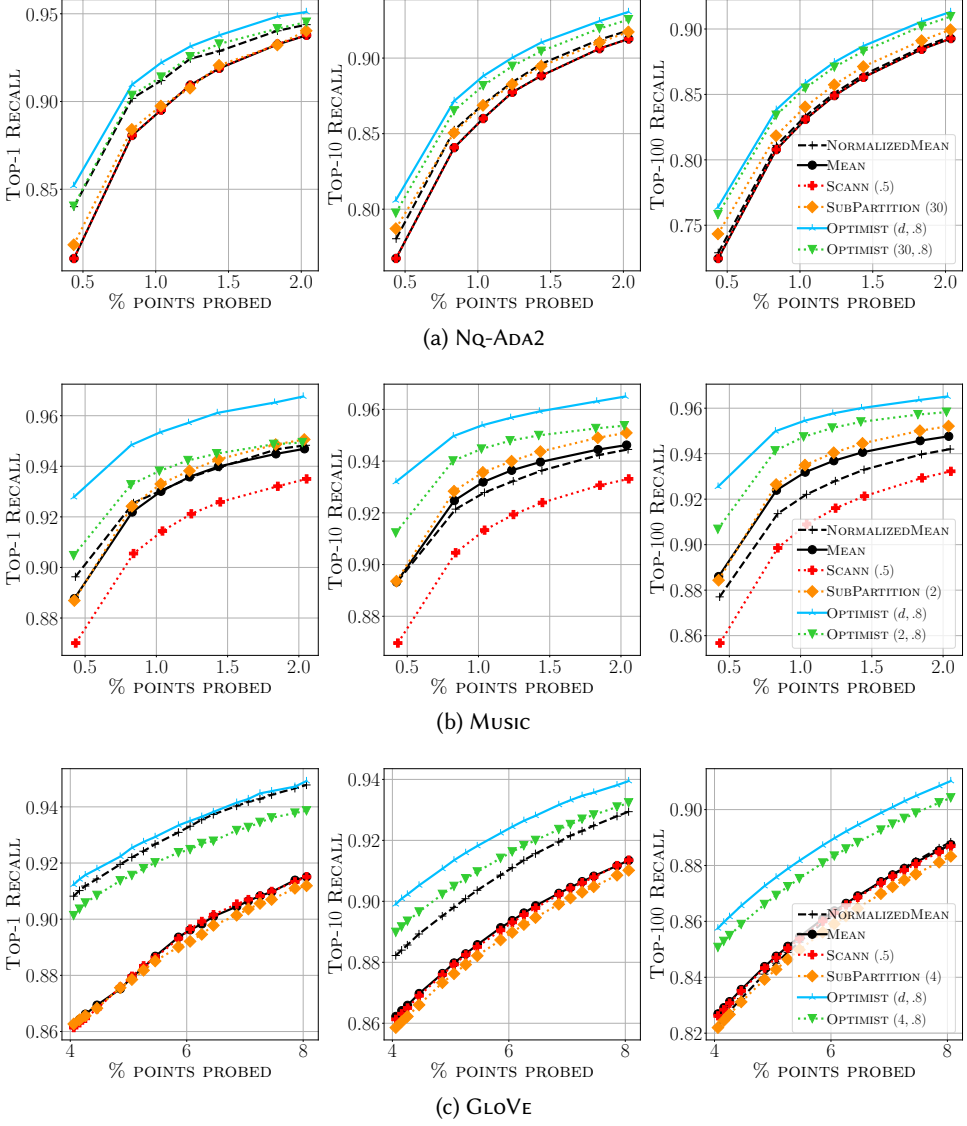


Fig. 10. Top- k recall vs. volume of probed data. Partitioning is with Standard KMeans. SCANN has parameter T , SUBPARTITION t (leading to $t + 2$ sub-partitions per shard), and OPTIMIST rank t and degree of optimism δ .

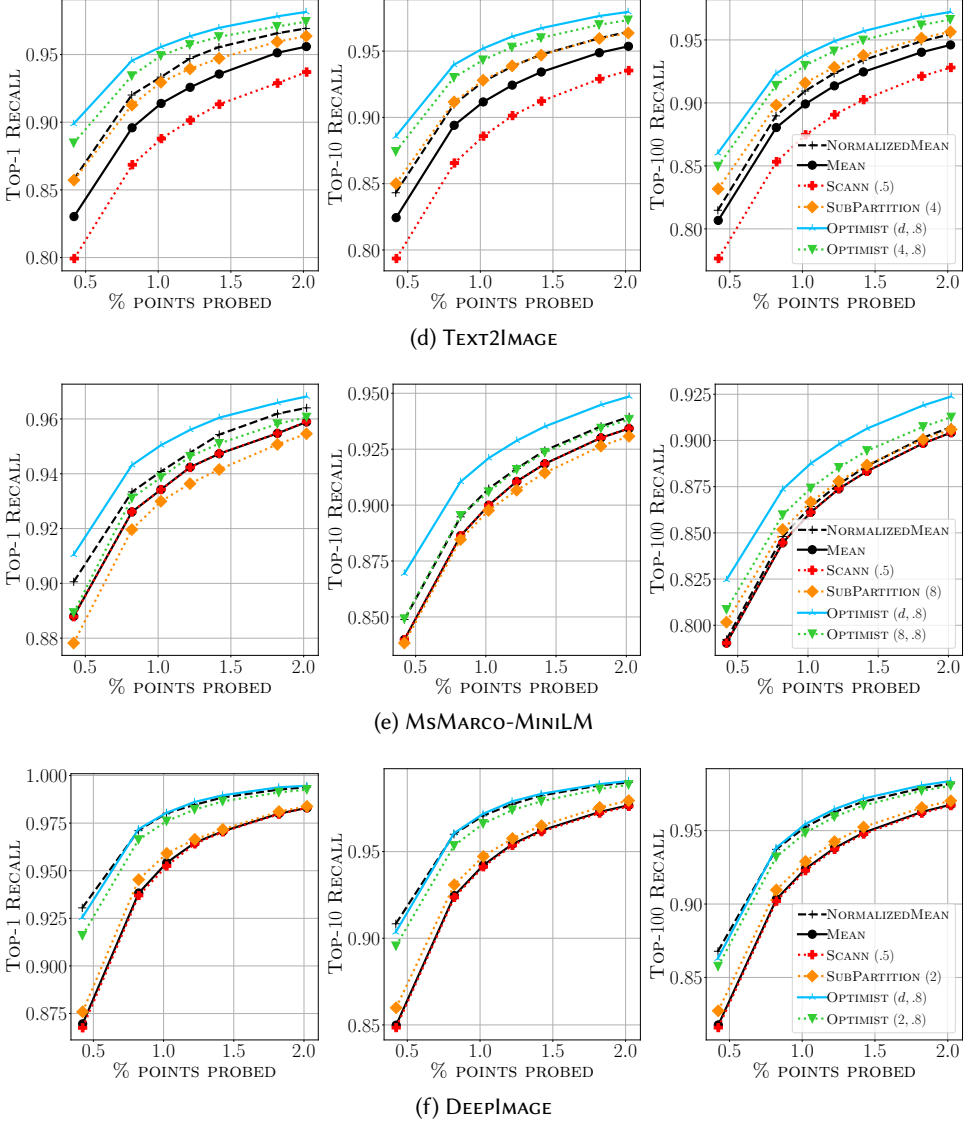


Fig. 10. Top- k recall vs. volume of probed data. Partitioning is with Standard KMeans. SCANN has parameter T , SUBPARTITION t (leading to $t + 2$ sub-partitions per shard), and OPTIMIST rank t and degree of optimism δ .

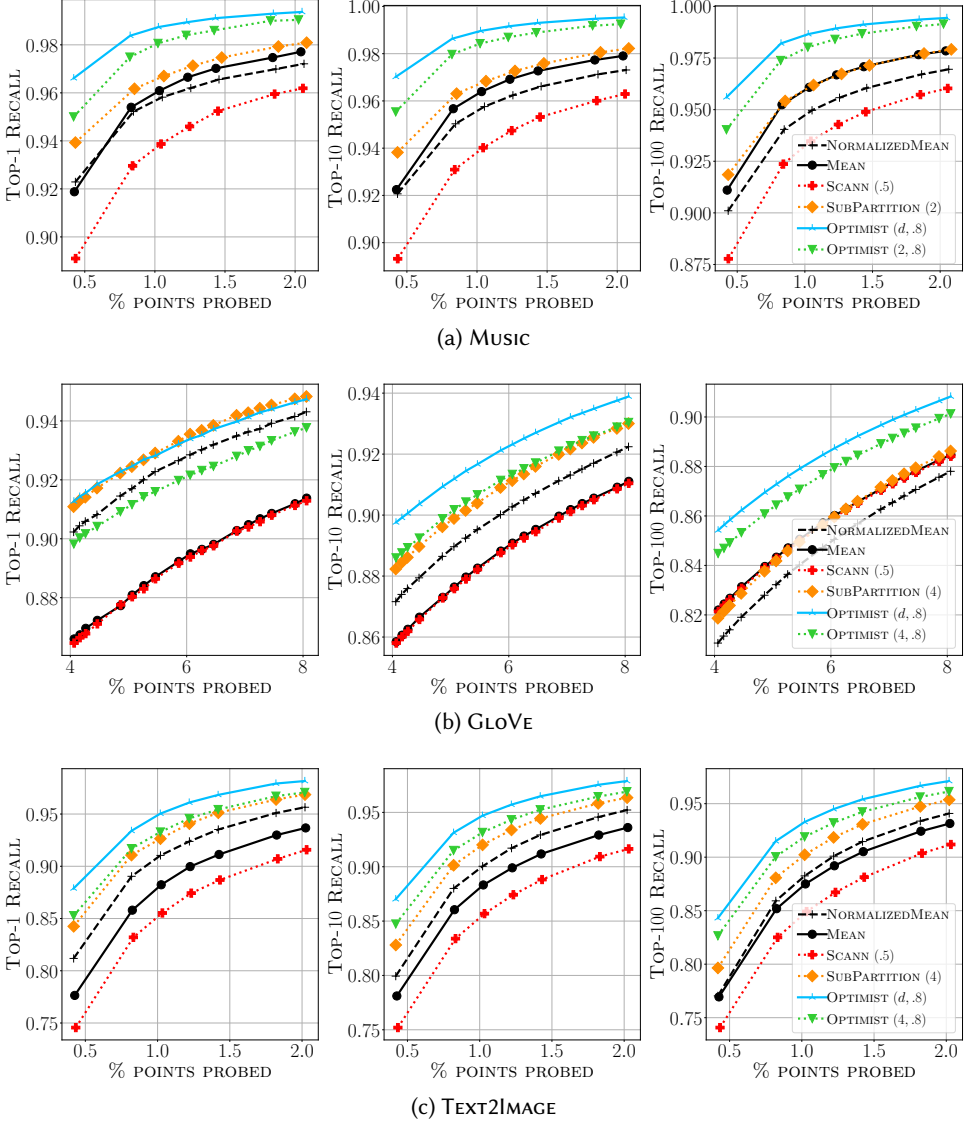


Fig. 11. Top- k recall vs. volume of probed data. Partitioning is with Gaussian Mixture Model. SCANN has parameter T , SUBPARTITION t (leading to $t + 2$ sub-partitions per shard), and OPTIMIST rank t and degree of optimism δ . We note that, due to the dimensionality of NQ-ADA2, we were unable to complete GMM clustering on this particular dataset.

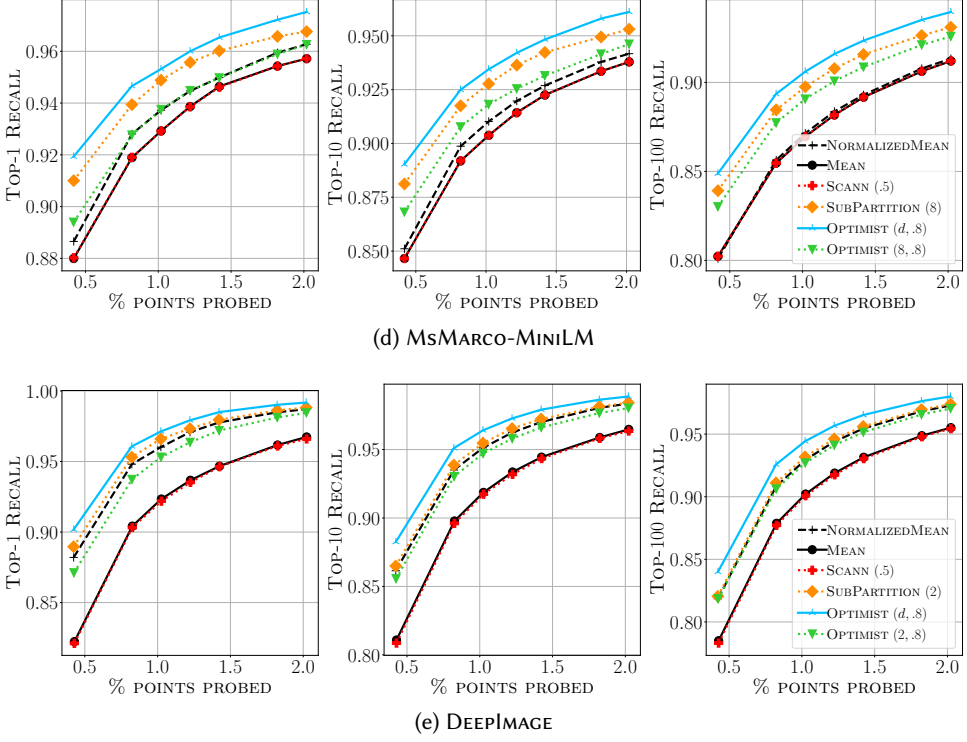


Fig. 11. Top- k recall vs. volume of probed data. Partitioning is with Gaussian Mixture Model. SCANN has parameter T , SUBPARTITION t (leading to $t + 2$ sub-partitions per shard), and OPTIMIST rank t and degree of optimism δ . We note that, due to the dimensionality of NQ-ADA2, we were unable to complete GMM clustering on this particular dataset.

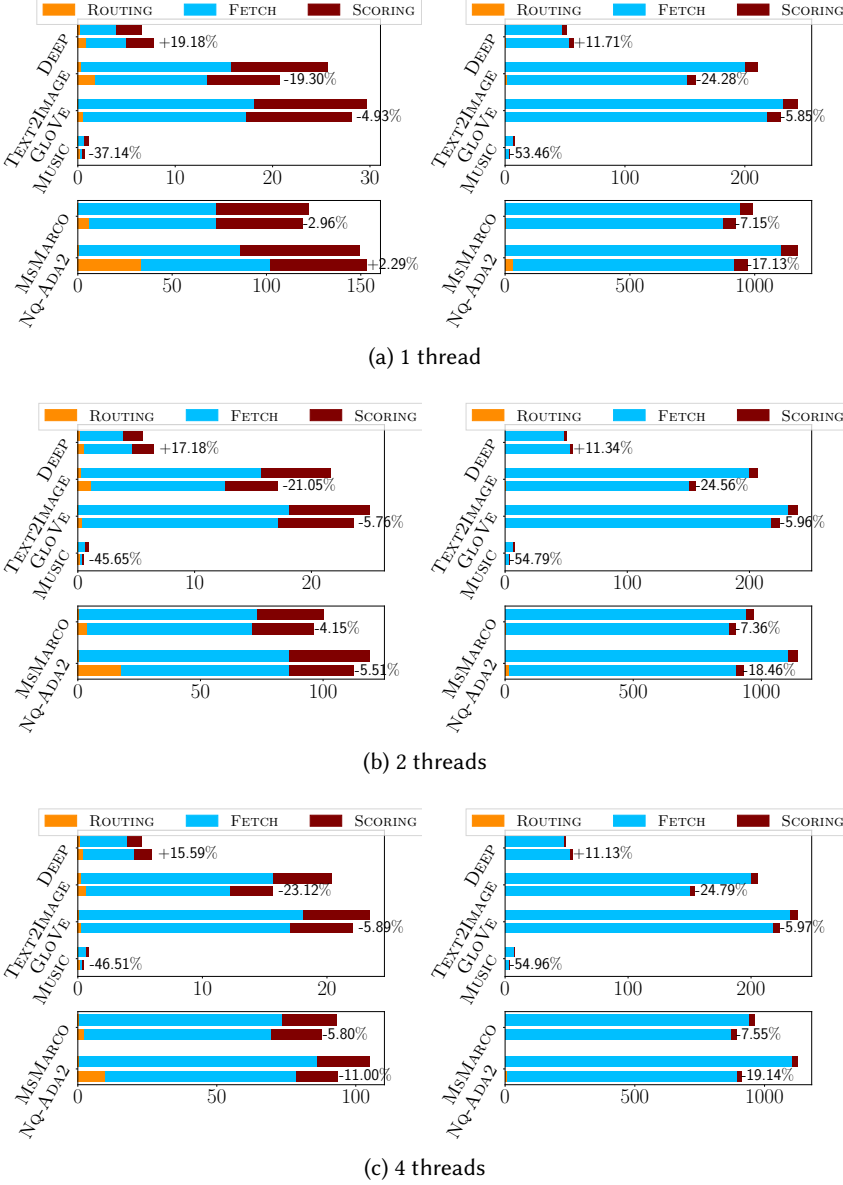


Fig. 12. Mean per-query latency (milliseconds) to reach 95% recall, using different number of threads, when data is stored on SSD (left column) and blob storage (right column). For each dataset, we plot the latency breakdown for NORMALIZEDMEAN (top bar) and OPTIMIST (bottom bar), and report relative gains (negative values indicate improvements, whereas positive values indicate losses) achieved by OPTIMIST with respect to NORMALIZEDMEAN. All shards are stored as PQ-compressed blobs using 4-dimensional codebooks—a common configuration.

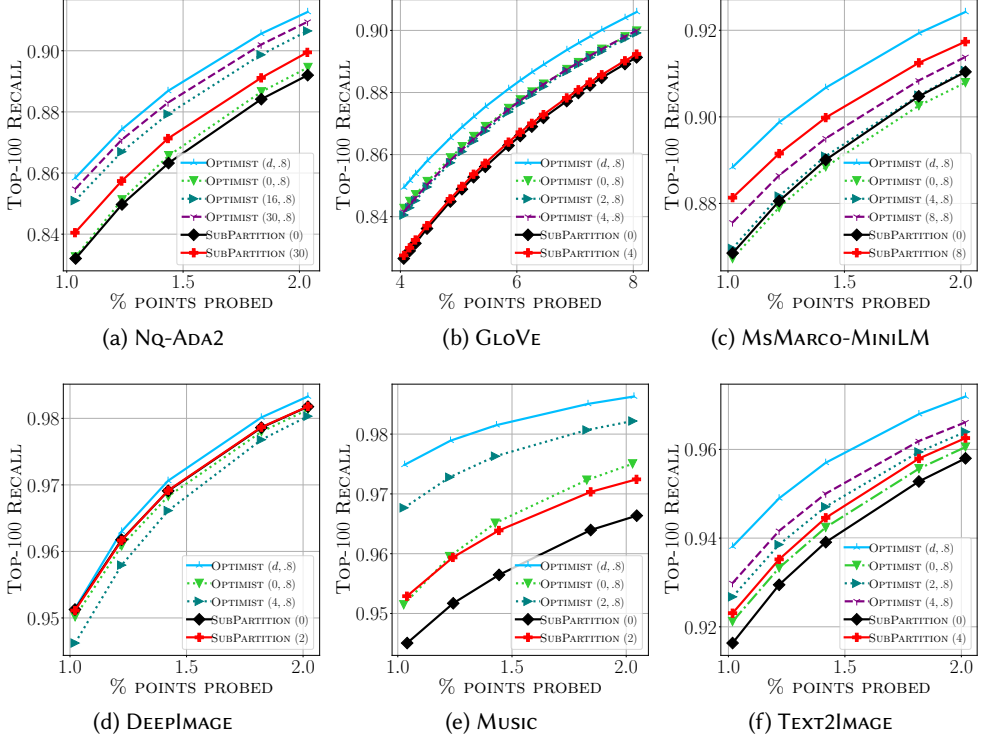


Fig. 13. Top-100 recall vs. volume of probed data as we change the rank of the covariance sketch (t). OPTIMIST(0, \cdot) denotes a sketch that only retains the diagonals. Partitioning is with Spherical KMeans.

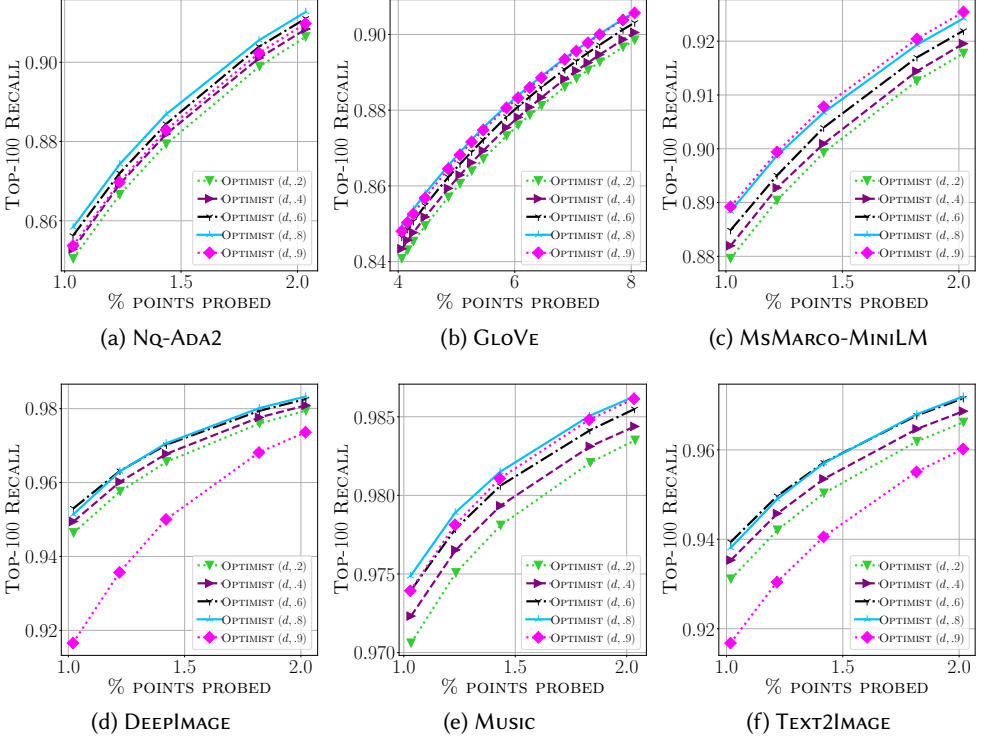


Fig. 14. Top-100 recall vs. volume of probed data, comparing a range of values of δ . As $\delta \rightarrow 1$, OPTIMIST becomes more optimistic. Partitioning is with Spherical KMeans.